MODELING AND CONTROL OF PROCESSES IN ORGANIC SOLAR CELLS

by

RAUNAK KUMAR

A thesis submitted to the

Graduate School-New Brunswick

Rutgers, The State University of New Jersey

In partial fulfillment of the requirements

For the degree of

Master of Science

Graduate Program in Electrical and Computer Engineering

Written under the direction of

Dr. Zoran Gajić

And approved by

_____

_____

_____

_____

New Brunswick, New Jersey

October, 2014

ABSTRACT OF THE THESIS

MODELING AND CONTROL OF PROCESSES IN ORGANIC SOLAR CELLS

by RAUNAK KUMAR

Thesis Director:

Dr. Zoran Gajić

The development of affordable, inexhaustible and clean solar energy technologies will have huge long term benefits, and the solar cell lies at the heart of this technology, which converts the incident sun light into electric current. During the last years the performance of bulk hetrojunction solar cells has been improved significantly making them a viable option for future generation solar cells. For a large-scale application of this technology further improvements are required.

In this thesis, we explore the means to improve the efficiency of organic solar cells by studying the one dimensional drift diffusion equations and understanding the parameters which play a significant role in the operations of these devices. After identifying the physical parameters, a state space technique is applied and the nonlinear model is developed which is both time and space varying. Then, two sub models are derived - one by freezing space and another by freezing time. Both models are nonlinear. We perform linearization of the nonlinear model around a nominal operating point for the purpose of designing linearized optimal controller. The controllers obtained are applied to the nonlinear solar cell model.

As the parameters are numerically very large in range, we performed scaling and derived a scaled down model. The internal stability of both the models is checked

and an optimal controller is developed around the nominal point with the objective to maintain a constant number of electrons and holes which in turn directly affects the output current of the solar cell. This steady state constant values can ensure desired charge separation which sweep towards the cathode and anode before they exit the device. In the event of high intensity of sunlight this steady state values will help overcome the space charge effect which is an important factor in organic cells.

The model is also subjected to the Turing instability test for a reaction diffusion system to investigate and detect the presence of Turing patterns in the drift-diffusion model of the organic solar cell.

Acknowledgements

First and foremost I express my deepest and sincerest gratitude to my adviser, Prof Zoran Gajić, who has supported me thoughout my dissertation with his guidance and patience.

His wide knowledge, constructive comments, and logical way of thinking have been of great value for me. Without his guidance and persistent help this thesis would not have been possible.

I would like to thank my committee members, Prof Sigrid McAfee and Prof Michael Caggiano. I also would like to thank faculty in Electrical and Computer Engineering Department for their help to get strong backgrounds for my research.

My deepest gratitude goes to my family for their unflagging love and support back home in India. This thesis is simply impossible without them.

Lastly, I offer my regards and blessings to all of those who supported me in any respect during the completion of the project.

Table of Contents

Chapter 1

Introduction

1.1 Overview

While a majority of the world's current electricity supply is generated from fossil fuels such as coal, oil and natural gas, these traditional energy sources face a number of challenges including rising prices, security concerns over dependence on imports from a limited number of countries which have significant fossil fuel supplies, and growing environmental concerns over the climate change risks associated with power generation using fossil fuels. As a result of these and other challenges facing traditional energy sources, governments, businesses and consumers are increasingly supporting the development of alternative energy sources and new technologies for electricity generation. Renewable energy sources such as fuel cell, solar cell, biomass, geothermal, hydroelectric and windpower generation have emerged as potential alternatives which address some of these concerns. As opposed to fossil fuels, which draw on finite resources that may eventually become too expensive to retrieve, renewable energy sources are generally unlimited in availability. Solar power generation has emerged as one of the most rapidly growing renewable sources of electricity, see Figure 1.1, Alon [2008].

Currently, the world consumes an average of 13 terawatts (TW) of power. By the year 2050, as the population increases and the standard of living in developing countries improves, this amount is likely to increase to 30 TW. If this power is provided by burning fossil fuels, the concentration of carbon dioxide in the atmosphere will more than double, causing substantial global warming, along with many other undesirable consequences. Therefore, one of the most important challenges facing engineers is finding a way to provide the world with 30 TW of power without releasing too much carbon into the atmosphere. Although it is possible that this could be done by using carbon

sequestration along with fossil fuels or by greatly expanding nuclear power plants, it is clearly desirable that we develop renewable sources of energy. The sun deposits 120,000 TW of radiation on the surface of the earth, so there is clearly enough power available if an efficient means of harvesting solar energy can be developed, [McGehee, 2008].

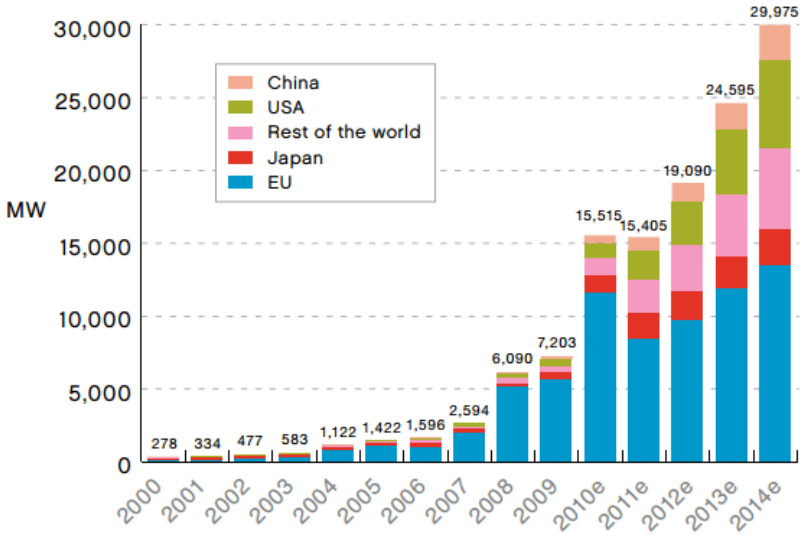

Figure 1.1: Global PV Market [EPIA, 2013]

Only a very small fraction of power today is generated by solar cells, which convert solar energy into electricity, because they are too expensive [Crabtree and Lewis, 2007]. More than 95 percent of the solar cells in use today are made of crystalline silicon (c-Si). The efficiency of the most common panels is approximately 10 percent, and the cost is $\$350/m^2$. In other words, the cost of the panels is $\$3.50/W$ of electricity produced in peak sunlight. When you add in the cost of installation, panel support, wiring, and DC to AC converters, the price rises to approximately $\$6/W$. Over the lifetime of a panel (approximately 30 years), the average cost of the electricity generated is $ 0.3/kW-hr. By comparison, in most parts of the United States, electricity costs about $ 0.06/kW-hr. Thus, it costs approximately five times as much for electricity from solar cells. If the cost of producing solar cells could be reduced by a factor of 10, solar energy would be not only environmentally favorable, but also economically favorable. Although c-Si solar cells will naturally become cheaper as economies of scale are realized, dicing and polishing wafers will always be somewhat expensive. Thus, it is desirable

that we find a cheaper way to make solar cells. The ideal method of manufacturing would be depositing patterned electrodes and semiconductors on rolls of plastic or metal in roll-to-roll coating machines, similar to those used to make photographic film or newspapers. Solar cells made this way would not only be cheaper, but could also be directly incorporated into roofing materials, thus reducing installation costs. Organic semiconductors that can be dissolved in common solvents and sprayed or printed onto substrates are very promising candidates for this application.

1.2 Thesis objective

The enormous gap between the potential of solar energy and our use of it is due to cost and conversion capacity. Dramatic cost-effective increases in the efficiency of solar energy conversion are enabled by our growing ability to understand and control the fundamental nanoscale phenomena that govern the conversion of photons into other forms of energy.

The powering of electronic devices is often limited to rigid and bulky energy solutions (such as batteries). The lack of thin, flexible, lightweight energy sources restricts innovations in application areas such as wireless, autonomous, and flexible systems. A small number of soft (polymer) batteries are newly available on the market; however, their small capacity implies frequent servicing. Although energy harvesting has the potential to provide supplementary or, in some cases, stand-alone continuous power, it inherently requires the matching of function and environment. Several lightweight, miniaturized energy-harvesting solutions have been demonstrated (such as microvibration energy harvesting), but most are extremely application specific, complex, expensive to manufacture, and ultimately still rigid.

Solar or light energy is abundant and is arguably the most accessible energy source for many electronics applications, as supplied by solar (also known as photovoltaic) cells. The performance of a solar cell is measured by power conversion efficiency (PCE) which is defined as the useful output power to the incident power. Silicon-based solar cells can typically achieve 20% in power conversion efficiency (PCE), but their high

manufacturing costs discourage greater use. In contrast, organic solar cells (OSCs) cost far less to manufacture because of the solution processable nature of their polymer ingredients. Polymers can be printed on thin, flexible substrates using roll-to-roll, ink-jet, or other print-based fabrication, avoiding costly siliconchip manufacturing equipment. Recent technological advances in OSCs have increased their PCE to higher than 8%. With the low manufacturing costs and increased PCE, OSCs now offer a very attractive, sub-dollar-per-watt production cost and are expected to greatly surpass silicon-based solar cells in price competitiveness.

The technology proposed in this thesis is based on the idea that efficiency of the organic solar cells can be improved considerbaly by controlling the number of electrons and the rate of flow of electrons in the organic solar cells across the device.

1.3 Conclusion

Based on the knowledge of recent growth in the need of solar technology and the recent advancements in the organic solar cells they are a very good candidate to research upon. The power concversion efficiency of these OSC if improved can play a major role in the future solar cell technology. In the next chapter 2 we investigate the different type of solar cells and their performance parameters.

Chapter 2

Evolution of Solar Cells

2.1 Photovoltaic Cells in Operation

2.1.1 Solar Cell Structure

A solar cell is an electronic device which directly converts sunlight into electricity. Light shining on the solar cell produces both a current and a voltage to generate electric power. This process requires firstly, a material in which the absorption of light raises an electron to a higher energy state, and secondly, the movement of this higher energy electron from the solar cell into an external circuit. The electron then dissipates its energy in the external circuit and returns to the solar cell. A variety of materials and processes can potentially satisfy the requirements for photovoltaic energy conversion, but in practice nearly all photovoltaic energy conversion uses semiconductor materials in the form of a p-n junction.

The basic steps in the operation of a solar cell are as follow :

1. The generation of light-generated carriers.
2. The collection of the light-generated carries to generate a current.
3. The generation of a large voltage across the solar cell.
4. The dissipation of power in the load and in parasitic resistances.

2.1.2 Traditional Model for Solar Cells

To understand the electrical behaviour of solar cells, it is useful to create an equivalent model for the traditional solar cell (shown in Figure 2.2). A solar cell, also known as

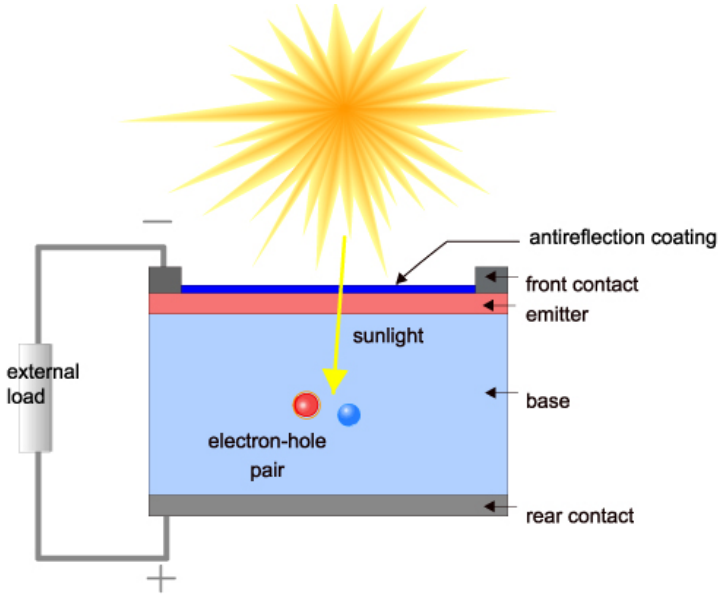

Figure 2.1: Cross section of a solar cell

a photodiode or photovoltaic, may be modeled by a current source in parallel with a diode (see Figure 2.2). The diode in the model represents a real physical diode which is created by the junction of P and N materials which form the solar cell. As photons strike the cells surface, they excite electrons and move them across the PN junction of the diode. Shunt and series resistances are added to obtain a better modeling of the current-voltage characteristic [Servaites *et al.*, 2011]. When the photovoltaic (PV) cell is illuminated and connected to a load a potential difference (V) appears across the load and a current (I) circulates. The cell functions as a generator as shown in Figure 2.2. The photons reaching the interior of the cell with energy greater than the band gap generate electron-hole pairs that may function as current carriers.

Some of these carriers will find themselves in or near the potential barrier and are accelerated as shown to form the photonic current. Other carriers will recombine and contribute to a diode or dark current as governed by the Shockley equation:

$$I_D = I_0(exp(-VD/mVT) - 1) \tag{2.1}$$

With:

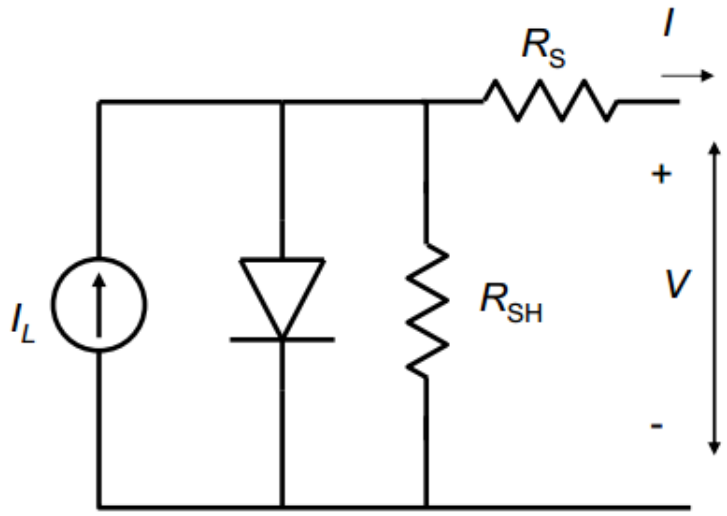

Figure 2.2: Circuit diagram for traditional solar cell

I_D : the diode current,

I_0 : the reverse bias saturation current (or scale current),

V_D : the voltage across the diode,

V_T : the thermal voltage,

m: the ideality factor, also known as the quality factor or sometimes emission coefficient. The ideality factor m varies from 1 to 2 depending on the fabrication process and semiconductor material and in many cases is assumed to be approximately equal to 1 (thus the notation m is omitted).

The thermal voltage V_T is approximately 25.85 mV at 300 K, a temperature close to "room temperature" commonly used in device simulation software. At any temperature it is a known constant defined by: $V_T = \frac{kT}{q}$, where k is the Boltzmann constant,T is the absolute temperature of the pn junction, and q is the magnitude of charge on an electron (the elementary charge), [Selwan, 2012]. The load current is the difference between the photonic and diode currents such that $I = I_v - I_D$, which when combined with Eq. 2.1 yields:

$$I = I_v - I_0(exp(-(V + IR_S)/mVT) - 1) \tag{2.2}$$

Note $V + IR_S = V_D$ and that the constant m= 1 at high current and m=2 at low

current.

The saturation current I_0 is difficult to measure and the I-V equation may be more usefully written in terms of the open-circuit voltage (V_{oc}) and the short circuit current (I_{sc}). The short circuit current is nearly equal to the photonic current $I \approx I_{sc}$ (RS is very small) and at open-circuit conditions reduces to:

$$0 = I_{sc} - I_0(exp(-(V_{oc})/V_T) - 1) \tag{2.3}$$

$\Longrightarrow$

$$V_{oc} = V_T ln(I_{sc}/I_0 + 1) \tag{2.4}$$

Thus we can conclude :

1. Series resistance causes ohmic loses.

2. Shunt resistance causes charge separated to recombine.

2.2 Model for Organic Solar Cells

The equivalent circuit diagram for the organic solar cell is shown in (Figure 2.3) [Iyer and Subramanian, 2007]. PV is modeled as a current source because it supplies a constant current over a wide range of voltages. This new model tries to model the circuit diagram by taking into account the inter-step excition formation in organic solar cells.

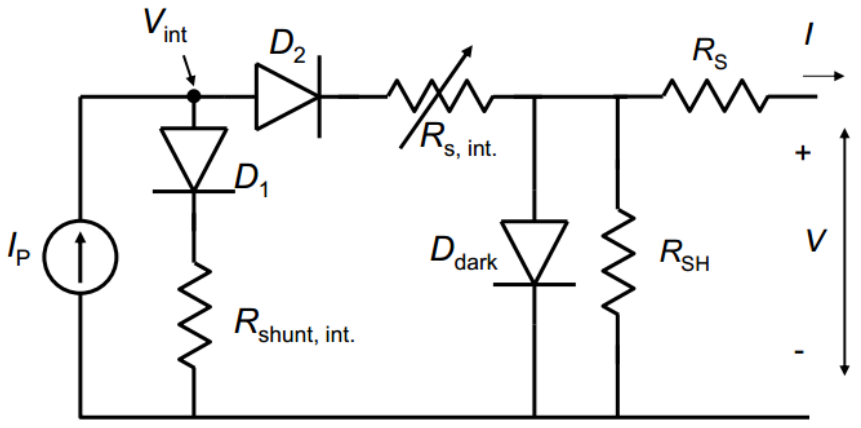

Figure 2.3: Circuit diagram for organic solar cell

The key features of this model are the following :

1. i is a function of voltage.
2. Exciton generation I_p is a constant.
3. $R_{shunt,int}$ will account for exciton recombination.
4. $R_{s,int}$ will account for extraction of e^- and h^+ to electrodes.

2.2.1 Control of Linear Time Varying Systems

The model as shown in Figure 2.3 has three diodes. As demonstrated in [Davoudi *et al.*, 2013] the diodes can be approximated by the second order linear time varying systems so that the circuit in Figure 2.3 can be modeled as a sixth order linear time varying system.

Studying linear time varying systems is numerically and analytically very challenging. Thus, we decided to follow the approach of developing state space model for drift diffuson model which is shown in next chapters.

2.3 Device Physics of the OPV Cell

General Working Principle

In OPV cells, the photovoltaic process of converting light to electricity is composed of four consecutive steps.

$$\eta_{eff} = \eta_{abs} \ * \ \eta_{diss} \ * \ \eta_{trans} \ * \ \eta_{col} \tag{2.5}$$

where :

η_{abs} : light absorption efficiency , η_{diss} : exciton dissociation efficiency,

η_{trans} : charge transport efficiency, η_{col} : charge collection efficiency

The first step is light absorption leading to exciton formation. When sunlight is directed onto photosensitive semiconducting organics, electrons in highest occupied molecular orbital (HOMO) are excited to lowest unoccupied molecular orbital

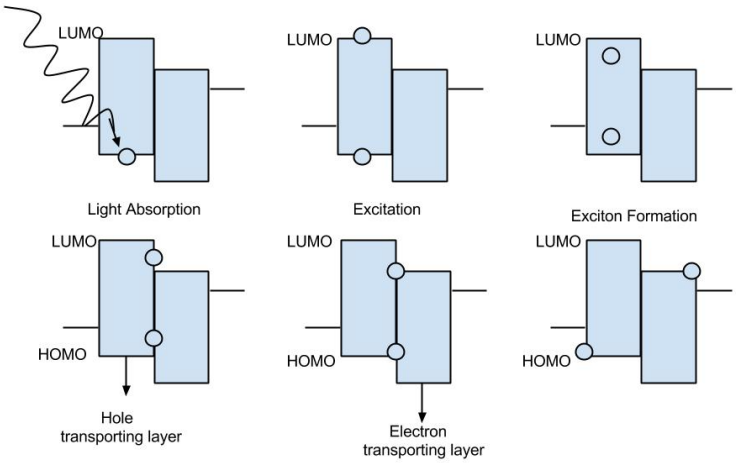

Figure 2.4: Device Working Principle from Light Absorption to Charge Collection

(LUMO). After light absorption, inorganic semiconductors immediately produce free carriers while organic semiconductors require additional processes to produce free carriers. First organic semiconductors form excitons, which are strongly bound electron-hole pairs, that then diffuse inside of the organic semiconductor, which is independent on an applied electric field. The typical exciton diffusion length in an organic semiconductor is around 10-20 nm, and exciton dissociation occurs only at the interface between the donor and the acceptor due to the offset of HOMO states of the donor and the acceptor [Arkhipov *et al.*, 2003]. If excitons do not reach the interface, they recombine and the absorbed energy is dissipated without generating photocurrent. Therefore, to efficiently generate power, the excitons have to be dissociated and collected at electrodes before recombination.The performance of an OPV cell is characterized by a J-V curve as seen below

The general current density and voltage characteristic under illumination are shown in Figure 2.5. and a electrical circuit of photovoltaic device is depicted in Figure 2.6. Under dark conditions, there is no current at the short circuit condition. Under an illumination condition, the incident photons generate current and the minus current

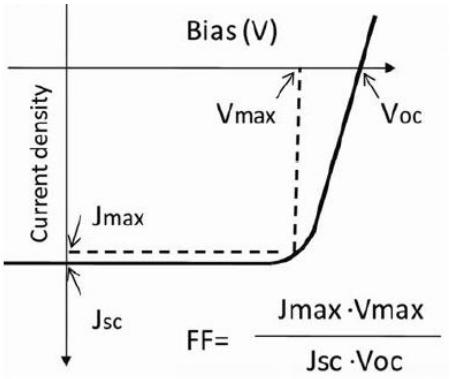

Figure 2.5: The definition of fill factor (FF), Jmax: current density at the maximum of J x V in 4th. quadrant, Vmax:bias at the maximum of J x V in 4th. Quadrant

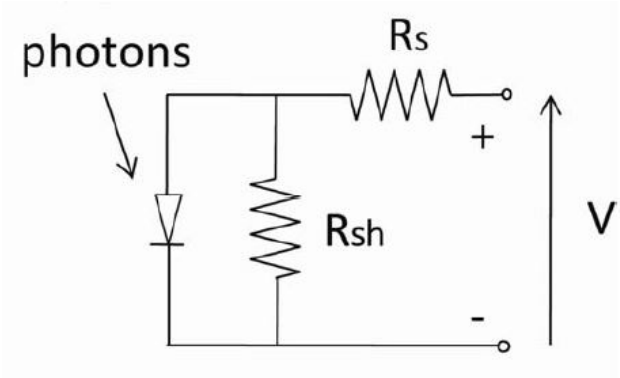

Figure 2.6: Circuit of photovoltaic device, Rs: series resistance, Rsh: shunt resistance.

density in the 4th quadrant of J-V curve indicates this photogenerated current. Parameters such as short circuit current (Jsc), open circuit voltage (Voc), fill factor (FF), and power conversion efficiency (PCE) are used to quantitatively analyze the performance of PV cells. For an ideal diode, the dark current density Jdark(V) is

$$J_{dark}(V) = J_o(e^{qV/k_BT} - 1) \tag{2.6}$$

where:

J_o is a constant,k_B is Boltzmanns constant and T is temperature in degrees Kelvin.

The overall current voltage response of the cell can be approximated as the sum of the short circuit photocurrent and the dark current. Although the reverse current, which flows in response to voltage in an illuminated cell, is not formally equal to the current that flows in the dark, the approximation is reasonable for many photovoltaic materials. The sign convention for current and voltage in photovoltaics is that the photocurrent

is negative. With this sign convention, the net current density in the cell is :

$$J_V = J_{dark}(V) - J_{sc} \tag{2.7}$$

which becomes for an ideal diode

$$J(V) = J_o(e^{qV/k_BT-1)} - J_{sc} \tag{2.8}$$

When the contacts are isolated, the potential difference has its maximum value, the open circuit voltage Voc. This is equivalent to the condition when the dark current and short circuit photocurrent exactly cancel out. For the ideal diode,

$$V_{oc} = \frac{kT}{q} ln(\frac{J_{sc}}{J_o} + 1) \tag{2.9}$$

Equation 2.4 shows that V_{oc} increases logarithmically with light intensity. Figure 2.5 shows that the current-voltage product is negative and the cell generates power when the voltage is between 0 and V_{oc}. At $V < 0$, the illuminated device acts as a photodetector, consuming power to generate a photocurrent that is light dependent but bias independent. At $V > V_{oc}$, the device again consumes power. This is the region where light emitting diodes operate.

Power Output and Fill Factor

The fill factor (FF) is calculated as

$$FF = \frac{J_m V_m}{J_{sc} V_{oc}} \tag{2.10}$$

to denote the part of the product of V_{oc} and J_{sc} that can be used. With this, the power conversion efficiency can be written as

$$\eta = \frac{P_{OUT}}{P_{IN}} = \frac{J_{MAX}V_{MAX}}{P_{IN}} = \frac{FFJ_{SC}V_{OC}}{P_{IN}} \tag{2.11}$$

When we consider parasitic resistances such as series resistance (Rs) and shunt resistance (Rsh), Equation(2.8) is modified as follows :

$$J(V) = J_o(e^{qV/k_BT} - 1) + \frac{V - JAR_s}{R_{sh}} - J_{sc} \tag{2.12}$$

In the real cell, power is dissipated through the resistance of the contacts and through leakage currents. These effects are equivalent electrically to two parasitic resistances in series (Rs) and in parallel (Rsh) (Figure 2.6). The series resistance arises from the resistance of the cell material to current flow, particularly through the front surface to the contacts. The parallel or shunt resistance arises from leakage of current through the cell. Since series and shunt resistances reduce fill factor, smaller Rs and larger Rsh are required in order to fabricate an efficient PV cell.

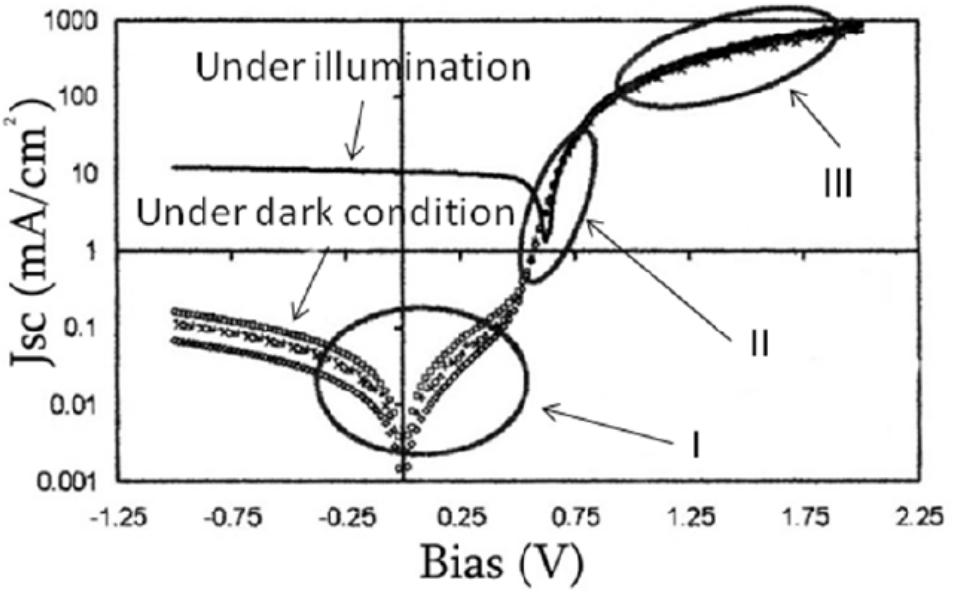

Figure 2.7: J-V curves under dark condition and illumination.y axis is log scale [Servaites *et al.*, 2011]

The derived Equation(2.8) includes comprehensive elements to explain the J-V curve of a PV cell. The y axis in Figure 2.7 is plotted in log scale and the J-V curve

has three regions that can be correlated with Rsh (region I), exponential behavior of pn junction (region II), and Rs (region III):

I. A linear regime at negative voltages and low positive voltages where the current is limited mainly by Rsh

II. An exponential behavior at intermediate positive voltages where the current is controlled by the diode

III. A second linear regime at high voltages where the current is limited by the Rs.

2.4 Scope to improve the efficiency of OSC

As the exciton binding energy in organic semiconductors is generally large (0.11eV) compared to silicon, the built-in electric fields (on the order of $10^6 - 10^7$V/m) are usually not high enough to dissociate the excitons directly. Hence, a process has to be introduced that efficiently separates the bound electron-hole pairs. This is possible at the sharp drop of potential at donor - acceptor (D-A) as well as semiconductor metal interfaces. A second issue is the consecutive charge transport to the electrodes.

Since $I = \frac{q}{t}$ and since $q = n * e$, this leads to :

1. By improving the number of electrons reaching the electrodes, more current can be extracted from the cell.

2. As $P_{out} = V * I$ thereby this can lead to an improve in efficiency for the cell at the given conditions.

2.5 Conclusion

In this chapter the two models : traditional model of solar cell and the organic solar cell model was introduced. The organic solar cell is an upcoming type of solar cell and their promising scope prompted us to learn more about the OSC. The power conversion efficiency and the fill factor was derived for the OSC. In the next chapter 3 we understand the parameters involved in the OSC and then model it into a state space form.

Chapter 3

Modeling and Control of Electron Hole Dynamics in Organic Solar Cell

The bulk hetrojunction solar cells has improved significantly in the last few years but for large scale applications of this technology further improvements are required which focuses in improving the power conversion efficiency of these cells. In this chapter, we will try to understand the physical parameters which factors out to play an important role in governing the operation of OSC (organic solar cells). In the second part of the chapter a state-space model is developed which is later on controlled to satisfy the control objective.

3.1 Understanding Physical Parameters of Organic Solar Cells

In order to optimize the power conversion efficiency (PCE) of these devices, we need to understand the factors playing important roles in the dynamics of photovoltaics. To qualify the loss mechanisms which are expected to occur we need to understand the distributions of the charge density and electric field in devices under various operating conditions.

In view of the above, we need to study the one-dimensional drift-diffusion equations which have successfully been used to model the steady state properties of bilayer and bulk hetrojunction devices [Hwang, 2008]. The internal nanaostructure of the active layer is ignored, and it is assumed that the device can be modelled by an effective medium approach with electron and hole mobilities μ_n and μ_p representing the transport of the respective carrier through the acceptor or donor component of the blend in the z direction. Denoting the electron, hole, and charge pair densities by n, p and X

respectively, the relevant equations are [Barker *et al.*, 2003] :

$$\frac{\partial n}{\partial t} = \frac{\partial}{\partial z}[-\mu_n k_B T \frac{\partial n}{\partial z} - \mu_n n e E] + k_{diss}(E)X - \gamma np \tag{3.1}$$

$$\frac{\partial p}{\partial t} = \frac{\partial}{\partial z}[-\mu_p k_B T \frac{\partial p}{\partial z} + \mu_p n e E] + k_{diss}(E)X - \gamma np \tag{3.2}$$

$$\frac{\partial E}{\partial z} = \frac{e(p-n)}{\epsilon_0 \epsilon_r} \tag{3.3}$$

$$\frac{\partial X}{\partial t} = G - k_{rec}X - k_{diss}(E)X - \gamma np \tag{3.4}$$

The paramters in the above partial differential equations (PDE) are the following :

n : electron density	p : hole density
ϵ_r: relative permittivity of material	ϵ_0 : absolute permittivity material
μ_n : electron mobility	μ_p : hole mobility
K_B : Boltzmann constant	E : electric field strength
K_{diss} : charge pair dissociation rate constant	X : charge pairs
K_{rec} : charge pair recombination rate constant	G: generation rate constant
e : elementary charge	T : absolute temperature

Equations (3.1) and (3.2) represent the coupled drift-diffusion equations for electrons and holes, with generation of free carriers by dissociation of charge pairs with the rate constant K_{diss}, and bimolecular recombination of electrons and holes to form charge pairs with the rate constant γ. Equation (3.3) represents the change in field inside the device due to space charges, and Equation (3.4) describes the dynamics of charge pairs which undergo molecular recombination with the rate constant K_{rec} and are generated wth rate G, which is assumed to be linearly proportional to the light intensity.

3.2 Developing a State Space Model for the Drift Diffusion Equations

Since the above PDE is both time and space varying we decided to do system analysis on both the varying qunatities separately by freezing one of them alternatively.

3.2.1 Freezing Space

Model obtained by freezing space :

$$\frac{\partial n}{\partial t} = k_{diss}(E)X - \gamma np \tag{3.5}$$

$$\frac{\partial X}{\partial t} = G - k_{rec}X - k_{diss}(E)X - \gamma np \tag{3.6}$$

In the above PDE we decide to choose the states as :

$$x_1 = n \qquad\qquad x_2 = X \tag{3.7}$$

The input variable chosen as the sunlight G

Thus the non linear state space quations will look like :

$$\dot{x_1} = k_{diss}(E)x - \gamma x_1^2 \tag{3.8}$$

$$\dot{x_2} = u - k_{rec}x_2 - k_{diss}(E)x_2 - \gamma x_1^2 \tag{3.9}$$

3.2.2 Freezing Time

Model obtained on freezing time based on differential equations for free carriers are as follows :

$$-\frac{1}{q}\frac{dJ_n}{dx} = -D_n\frac{d^2n}{dx^2} - F\mu_n\frac{dn}{dx} = g - k_{rec}np; \tag{3.10}$$

$$-\frac{1}{q}\frac{dJ_p}{dx} = -D_p\frac{d^2p}{dx^2} + F\mu_p\frac{dp}{dx} = g - k_{rec}np; \tag{3.11}$$

Thus we have the following equations :

$$-D_n\frac{d^2n}{dx^2} - F\mu_n\frac{dn}{dx} = g - k_{rec}np \tag{3.12}$$

$$-D_p\frac{d^2p}{dx^2}+F\mu_p\frac{dp}{dx}=g-k_{rec}np \tag{3.13}$$

In the above PDE we decide to choose the states as :

$$x_1=n \qquad\qquad x_2=\frac{\partial n}{\partial t} \tag{3.14}$$

$$x_3=p \qquad\qquad x_4=\frac{\partial p}{\partial t} \tag{3.15}$$

Thus we get the state equations as :

$$\dot{x}_1=x_2 \tag{3.16}$$

$$\dot{x}_2=-\frac{F}{D_n}\mu_n x_2-\frac{g}{D_n}+\frac{k_{rec}}{D_n}x_1x_3 \tag{3.17}$$

$$\dot{x}_3=x_4 \tag{3.18}$$

$$\dot{x}_4=-\frac{F}{D_p}\mu_p x_4-\frac{g}{D_p}+\frac{k_{rec}}{D_p}x_1x_3 \tag{3.19}$$

3.3 Control of Nonlinear Systems via Linearization

As we notice that both the 2nd order and 4th order models are nonlinear, there is a need to linearize the system around a nominal operating point which best replicates the non linear system. The sytem around this operating point will be a linearized version of the nonlinear system. Thus, there arises a need to come up with a control strategy to achieve our goal for this linearized system.

The model we have developed is a nonlinear model, thus we use the approach of controlling nonlinear systems via linearization, by [Friedland, 1985] and [Gajic, 2003]. This approach is summarized below :

Given a non linear system

$$\dot{x}=f(x,u) \tag{3.20}$$

$$y=g(x,u) \tag{3.21}$$

where $x\,\epsilon R^n$ are state variables, $u\,\epsilon R^m$ are control output, $y\,\epsilon R^l$ is the system output and f, g are nonlinear functions.

Assuming that the system nominal points (operation point) often the steady state point is known, that is

$$x_{nom}\,, u_{nom}\,, y_{nom} = y_{desired} \text{ are known} \tag{3.22}$$

and that the system operates in the neighborhood of it's nominal point, that is

$$x(t) = x_{nom} + \triangle x(t) \tag{3.23}$$

$$u(t) = u_{nom} + \triangle u(t) \tag{3.24}$$

$$y(t) = y_{nom} + \triangle y(t) \tag{3.25}$$

$\triangle x(t)$, $\triangle u(t)$, $\triangle y(t)$ are small quantities.

Then, the system can be linearized around its nominal points leading to a linear system for $\triangle x(t)$, $\triangle u(t)$ and $\triangle\, y(t)$

$$\triangle\, \dot{x}(t) = A \triangle\, x(t) + B \triangle\, u(t) \tag{3.26}$$

$$\triangle\ \ y(t) = C \triangle\, x(t) + D \triangle\, u(t) \tag{3.27}$$

where

$$A = \frac{\partial f}{\partial x}_{|x_{nom},u_{nom}} \qquad B = \frac{\partial f}{\partial u}_{|x_{nom},u_{nom}} \tag{3.28}$$

$$C = \frac{\partial g}{\partial x}_{|x_{nom},u_{nom}} \qquad D = \frac{\partial g}{\partial u}_{|x_{nom},u_{nom}} \tag{3.29}$$

Since the above is a linear system, we can use any linear controller design technique to control $\triangle x(t)$ via $\triangle u(t)$.

In most cases, the nominal points are the steady state points which can be obtained from

$$0 = f(x_{nom}, u_{nom}) \tag{3.30}$$

$$y_{nom} = y_{desired} = g(x_{nom}, u_{nom}) \tag{3.31}$$

Now since $x_{nom}\, u_{nom}\,,\ y_{nom}$ are known, in general from the above set of equations we can obtain the relationship

$$u_{nom} = \varphi(x_{nom}, y_{nom}) \tag{3.32}$$

which is called the set-point controller.

Also we need to obtain

$$x_{nom} = \varphi(u_{nom}, y_{nom}) \tag{3.33}$$

Since the goal is to reduce $\triangle \mathbf{x(t)} \rightarrow \mathbf{0}$ and bring the system back to it's nominal trajectory (in which case $\triangle u(t) \rightarrow 0$ and $\triangle y(t) \rightarrow 0$ so that $y(t) \rightarrow y_{desired} = y_{nom}$) we can design any linear controller using the above derived linear system to achieve that task. We can now use any linear controller design technique to get the signal $\triangle u(t)$ from $\triangle x(t)$.

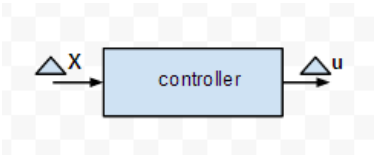

Figure 3.1: Linear Controller

The corresponding block diagram for controlling a non linear system via linearization is presented in Figure 3.2. It is adapted from [Friedland, 1985].

The block diagram can be implemented in Simulink as follows :

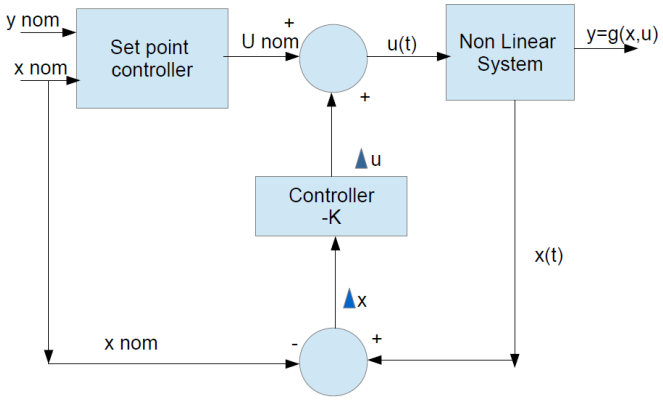

Figure 3.2: Control of non linear systems via linearization

3.4 Linearizing the Nonlinear System

The usual practice is to linearize the nonlinear system

$$\dot{x}_1(t) = x_2(t) \tag{3.34}$$

$$\dot{x}_2(t) = -\frac{F}{D_n}\mu_n x_2(t) - \frac{g}{D_n} + \frac{k_{rec}}{D_n}x_1(t)x_3(t) \tag{3.35}$$

$$\dot{x}_3(t) = x_4(t) \tag{3.36}$$

$$\dot{x}_4(t) = -\frac{F}{D_p}\mu_p x_4(t) - \frac{g}{D_p} + \frac{k_{rec}}{D_p}x_1(t)x_3(t) \tag{3.37}$$

around it's equilibrium points

$$0 = x_2^{ss} \tag{3.38}$$

$$0 = -F\mu_n x_2^{ss} - g + k_{rec}x_1^{ss}x_3^{ss} \tag{3.39}$$

$$0 = x_4^{ss} \tag{3.40}$$

$$0 = -F\mu_p x_4^{ss} - g + k_{rec}x_1^{ss}x_3^{ss} \tag{3.41}$$

Substituting equation (4.5) in equation (4.6) and substituting equation (4.7) in equation (4.8) we get :

$$K_{rec} x_1^{ss} x_3^{ss} - g = 0 \tag{3.42}$$

which leads to

$$x_1^{ss} = \frac{g}{K_{rec}} \frac{1}{x_3^{ss}} \tag{3.43}$$

This implies :

$$x_1^{ss} \propto \frac{1}{x_3^{ss}} \tag{3.44}$$

which is incorrect as the number of electrons generated cannot be inversely proportional to the number of holes generated.

Thus, linearzing the non linear system about the origin does not seem to be correct. We will further see in the next chapter the choice of the nominal point around which this system is linearized.

3.5 System Analysis of the Model

The goal for this model is to have the desired number of electrons present in the solar cell as the sunlight strikes the cell because we believe that the output current depends on the rate of flow of elctrons in the cell and more the electrons, more is the current.

$$i.e.\ y = y_{desired} = n = x_1 \tag{3.45}$$

3.5.1 2nd Order Model

Now as we see that our model is nonlinear we will like to have a linear controller to control $u(t)$ around the steady state.

So let us linearize the system at steady state :

$$0 = k_{diss}(E) x_2^{ss} - \gamma x_1^{2ss} = f_1(x_1^{ss}, x_2^{ss}) \tag{3.46}$$

$$0 = u - k_{rec}x_2^{ss} - k_{diss}(E)x_2^{ss} - \gamma x_1^{2ss} = f_2(x_1^{ss}, x_2^{ss}) \tag{3.47}$$

$$y^{ss} = y_{desired} = x_1^{ss} \tag{3.48}$$

For this linear model we will calulate the system matrix by calculating the Jacobian matrix which is given by :

$$\begin{bmatrix} \frac{\partial f_1}{\partial x_1} & \frac{\partial f_1}{\partial x_2} \\ \frac{\partial f_2}{\partial x_1} & \frac{\partial f_2}{\partial x_2} \end{bmatrix}. \tag{3.49}$$

Thus the system state space matrices are as follows :

$$A = \begin{bmatrix} -2\gamma x_1 & k_{diss}(E) \\ -2\gamma x_1 & -(k_{rec} + k_{diss}(E)) \end{bmatrix} \tag{3.50}$$

$$B = \begin{bmatrix} 0 \\ 1 \end{bmatrix} \tag{3.51}$$

$$C = \begin{bmatrix} 1 & 0 \end{bmatrix} \tag{3.52}$$

$$D = 0 \tag{3.53}$$

Before moving further and design the controller we decided to check the internal stability of the system and thus we have applied the Routh Hurwitz crietrion.

Considering the system matrix A to be generalized now :

$$A = \begin{bmatrix} a & b \\ a & d \end{bmatrix} \tag{3.54}$$

Thus,

$$\text{poly(A)} = x^2 + (-a - c)x - ab + ac \tag{3.55}$$

Formulating the Routh's table we get :

$$\begin{aligned} s^2 &: \ 1 && a(c-b) \\ s^1 &: \ (-a-c) && 0 \\ s^0 &: (ac + ab) \end{aligned}$$

Now as we know according to Routh's criteria for a system to be stable there should be no sign changes in the first column of the Routh's table

Therefore, we get :

$$1)\ (-a-c)>0 \quad \Longrightarrow \quad a+c<0 \tag{3.56}$$

$$2)\ -ac+ab>0 \quad \Longrightarrow \quad a(c-b)>0 \tag{3.57}$$

which leads to :

$$b>c \ \ if \quad a>0 \tag{3.58}$$

and

$$b<c \quad if \quad a<0 \tag{3.59}$$

Now since,

$$a=-2\gamma x_1 \Longrightarrow a<0 \tag{3.60}$$

and as

$$b=k_{diss}(E)\ and\ c=-(k_{rec}+k_{diss}(E)) \implies b>c \tag{3.61}$$

Therefore the system is asymptotically stable.

3.5.2 4th Order Model

Model obtained on freezing time based on differential equations for free carriers which are as follows :

$$-\frac{1}{q}\ \frac{dJ_n}{dx}=-D_n\ \frac{d^2n}{dx^2}-F\mu_n\frac{dn}{dx}=g-k_{rec}np; \tag{3.62}$$

$$-\frac{1}{q}\ \frac{dJ_p}{dx}=-D_p\ \frac{d^2p}{dx^2}+F\mu_p\frac{dp}{dx}=g-k_{rec}np; \tag{3.63}$$

Thus on freezing time, we have the following equation :

$$-D_n\frac{d^2n}{dx^2}-F\mu_n\frac{dn}{dx}=g-k_{rec}np \tag{3.64}$$

$$-D_p\frac{d^2p}{dx^2}+F\mu_p\frac{dp}{dx}=g-k_{rec}np \tag{3.65}$$

In the above PDE, we decide to choose the states as :

$$x_1 = n \tag{3.66}$$

$$x_2 = \frac{\partial n}{\partial t} \tag{3.67}$$

$$x_3 = p \tag{3.68}$$

$$x_4 = \frac{\partial p}{\partial t} \tag{3.69}$$

Thus, we get the state equations as :

$$\dot{x}_1(t) = x_2(t) \tag{3.70}$$

$$\dot{x}_2(t) = -\frac{F}{D_n}\mu_n x_2(t) - \frac{g}{D_n} + \frac{k_{rec}}{D_n}x_1(t)x_3(t) \tag{3.71}$$

$$\dot{x}_3(t) = x_4(t) \tag{3.72}$$

$$\dot{x}_4(t) = -\frac{F}{D_p}\mu_p x_4(t) - \frac{g}{D_p} + \frac{k_{rec}}{D_p}x_1(t)x_3(t) \tag{3.73}$$

For this linear model, we will calulate the system matrix by calculating the Jacobian matrix which is given by :

$$\begin{bmatrix} \frac{\partial f_1}{\partial x_1} & \frac{\partial f_1}{\partial x_2} & \frac{\partial f_1}{\partial x_3} & \frac{\partial f_1}{\partial x_4} \\ \frac{\partial f_2}{\partial x_1} & \frac{\partial f_2}{\partial x_2} & \frac{\partial f_2}{\partial x_3} & \frac{\partial f_2}{\partial x_4} \\ \frac{\partial f_3}{\partial x_1} & \frac{\partial f_3}{\partial x_2} & \frac{\partial f_3}{\partial x_3} & \frac{\partial f_3}{\partial x_4} \\ \frac{\partial f_4}{\partial x_1} & \frac{\partial f_4}{\partial x_2} & \frac{\partial f_4}{\partial x_3} & \frac{\partial f_4}{\partial x_4} \end{bmatrix}. \tag{3.74}$$

Thus the system matrices are as follows :

$$A = \begin{bmatrix} 0 & 1 & 0 & 0 \\ \frac{k_{rec}}{D_n}x_3^{nom} & \frac{-F}{D_n}\mu_n & \frac{k_{rec}}{D_n}x_1^{nom} & 0 \\ 0 & 0 & 0 & 1 \\ \frac{k_{rec}}{D_p}x_3^{nom} & 0 & \frac{k_{rec}}{D_p}x_1^{nom} & \frac{F}{D_p}\mu_p \end{bmatrix} \tag{3.75}$$

$$B = \begin{bmatrix} 0 \\ -\frac{1}{D_n} \\ 0 \\ -\frac{1}{D_p} \end{bmatrix} \tag{3.76}$$

$$C = \begin{bmatrix} 1 & 0 & 0 & 0 \end{bmatrix} \tag{3.77}$$

$$D = 0 \tag{3.78}$$

Routh Hurwitz's Stability Test for 4th Order Model

For the system matrix as shown in Equation (3.79) we need to check the asymptotic stability and which is done by applying the Routh Hurwitz's stability test.

The matrix can be represented conveniently as the following :

$$A = \begin{bmatrix} 0 & 1 & 0 & 0 \\ ax_3^{nom} & -c & ax_1^{nom} & 0 \\ 0 & 0 & 0 & 1 \\ bx_3^{nom} & 0 & bx_1^{nom} & d \end{bmatrix} \tag{3.79}$$

The characteristic equation of the system can be calculated as the following : $\left|\lambda I - A\right| = \det(\lambda I - A)$

$$= \begin{bmatrix} \lambda & 0 & 0 & 0 \\ 0 & \lambda & 0 & 0 \\ 0 & 0 & \lambda & 0 \\ 0 & 0 & 0 & \lambda \end{bmatrix} - \begin{bmatrix} 0 & 1 & 0 & 0 \\ ax_3^{nom} & -c & ax_1^{nom} & 0 \\ 0 & 0 & 0 & 1 \\ bx_3^{nom} & 0 & bx_1^{nom} & d \end{bmatrix}$$

$$= \begin{bmatrix} \lambda & -1 & 0 & 0 \\ -ax_3^{nom} & \lambda + c & -ax_1^{nom} & 0 \\ 0 & 0 & \lambda & -1 \\ -bx_3^{nom} & 0 & -bx_1^{nom} & \lambda - d \end{bmatrix}$$

Now to calcualte the determinant of the above matrix we can expand it along row 1 and after which we get :

$$\lambda^4 + \lambda^3[c-d] + \lambda^2[-bx_1^{nom} - cd - ax_3^{nom}] + \lambda[adx_3^{nom} - bcx_1^{nom}] = 0 \tag{3.80}$$

Now forming the Routh's array we get :

$s^4 :$ 1 $\quad (-bx_1^{nom} - cd - ax_3^{nom}) \quad 0$

$s^3 : (c-d)(adx_3^{nom} - bcx_1^{nom}) \quad 0$

$s^2 : \frac{(c-d)(-bx_1^{nom} - cd - ax_3^{nom} - (adx_3^{nom} - bcx_1^{nom})}{(c-d)} \quad 0 \quad 0$

$s^1 : (adx_3^{nom} - bcx_1^{nom}) \quad 0$

$s^0 : 0$

Condition for stability :

There should be no sign changes in the first column of the Routh's array. We get the following conditions :

$$c - d > 0 \tag{3.81}$$

In other words, $\mu_n > \mu_p$ which is true for our model.

$$(adx_3^{nom} - bcx_1^{nom}) > 0 \tag{3.82}$$

which is equivalent to :

$$adx_3^{nom} > bcx_1^{nom} \tag{3.83}$$

Since, $\mu_n > \mu_p$ thus for this condition to hold true $x_3^{nom} > x_1^{nom}$ i.e holes > electrons. This result is in tune with the results we display for the simulation of our model.

3.6 LQR Controller Design

One way of finding K_c is by using the Linear-Quadratic Regulator (LQR) design. We will state the problem as follows:

Consider the system

$$\dot{x}(t) = Ax(t) + Bu(t), x(0) = x_0 \tag{3.84}$$

We seek a control $u^*(t)$ that minimizes the performance measure

$$\min_u J = \int_0^\infty [(\mathrm{Qx(t), x(t)}) + (\mathrm{Ru(t), u(t)})]\, \mathrm{d}t \tag{3.85}$$

where $x(t)$ is the solution of the above system equation: Here $Q = Q^T \geq 0$ and $R = R^T > 0$ are weighting matrices. It is well known that if an optimal control $u^*(t)$ exists, it has the form

$$u^*(t) = -K_c x(t) \tag{3.86}$$

where K_c is a constant gain matrix. Moreover, the closed loop system

$$\dot{x}(t) = Ax(t) - BK_c x(t) = (A - BK_c)x(t) \tag{3.87}$$

is asymptotically stable. The assumption that $R > 0$ ensures that the energy of the control is finite. The following result may be found in [Dorato *et al.*, 2000].

Existence and Stability of the Steady-State LQR Solution :

Given the LQR problem with $R > 0$, and $Q = C^T C$, where the pair (A, C) is detectable and the pair (A, B) is stabilizable, it follows that the solution to the steady-state LQR problem exists. In particular, there exists a unique positive semidefinitive solution $\bar{P}$ to the algebraic Riccati equation [Hwang *et al.*, 2010].

$$0 = A^T P + PA + Q - PBR^{-1}B^T P \tag{3.88}$$

and

$$K_c = R^{-1}B^T \bar{P} \tag{3.89}$$

make the closed loop system (3.87) is asymptotically stable. The simulation results for this controller will be presented in the next chapter.

3.7 Conclusion

In this chapter, we modelled the OSC which is both time and space varying into two sub models. We also investigated their internal stability using the Routh Hurwitz stability test and found them to be asymptotically stable. Thus based on this, we proposed an optimal LQR and a set point controller to achieve our control goal. In the next chapter 4 we will see the results from simulating the models in MATLAB.

Chapter 4

Observations and Results

The electric current that a photovoltaic solar cell delivers corresponds to the number of created charges that are collected at the electrodes. As discussed in Equation(2.5), this number depends on the fraction of photons absorbed (η_{abs}), the fraction of electron-hole pairs that are dissociated (η_{diss}), and finally the fraction of (separated) charges that reach the electrodes (η_{col}) determining the overall photocurrent efficiency(η_{eff}).

The fraction of absorbed photons is a function of the absorption spectrum, absorption coefficient, absorbing layer thickness, and of internal multiple reflections at, for example, metallic electrodes. The fraction of dissociated electron-hole pairs on the other hand is determined by whether they diffuse into a region where charge separation occurs and on the charge separation probability there. To reach the electrodes, the charge carriers need a net driving force which generally results from a gradient in the electrochemical potentials of electrons and holes.

4.1 Frozen Space

In our submodel of frozen space we demonstrate that we examine the number of electrons and the charge pairs as to how they can effect the organic solar cell with change in time eventually playing a vital role in the pheonomenon like state space charge recombination and high electric field dissociation.

4.1.1 Data

The values of the parameters used to simulate the formulated model was obtained from [Barker *et al.*, 2003], [Hwang, 2008] and [Kirchartz *et al.*, 2008] :
$\gamma = 3 * 10^{-4} m^{1/2} V^{-1/2}$, $K_{rec} = 10^3\, s^{-1}$, $K_{diss} = 10^5\, s^{-1}$, $n = 8 * 10^{10} m^{-3}$

4.1.2 2nd Order : Block Diagram

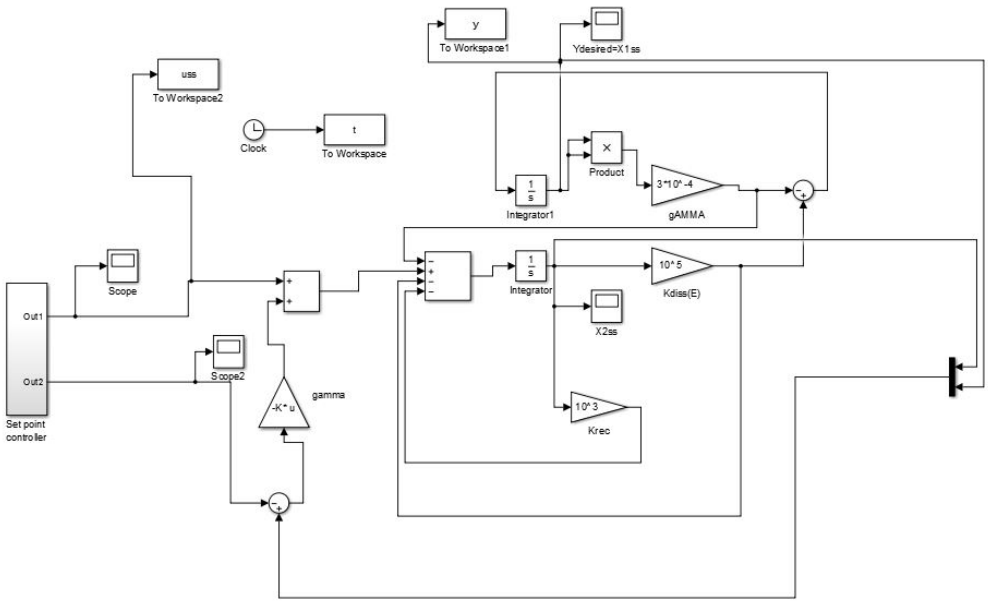

Figure 4.1: 2nd order nonlinear organic solar cell model implemented in Simulink

Figure 4.1 is a block diagram representation of the 2nd order solar cell model in Simulink wherein a set-point controller as shown in Figure 4.2 is used to control the number of electrons and the charge pairs as they vary in time. The charge pairs is given by $X = \frac{\gamma n^2}{k_{diss}}$ and thus controlling the number of electrons also affects the charge pair densitiy in the model.

4.1.3 Scaled Down Model

The system matrix as represnted in Equation(3.50) is of the order of magnitude 10^{21}. MATLAB gives precision errors when the optimal control algorithm is applied, thus we need to scale down the model.

The scaled down variables are :

$\hat{x}_1 = 10^{-5} * x_1$

$\hat{x}_2 = 10^{10} * x_2$

$\hat{u} = 10^{10} * u_{ss}$;

And now the order of magnitude reduces to order 10^7 which is manageable in order to control. Also, the scaled down model is both controllable and observable.

4.1.4 Set-point Controller

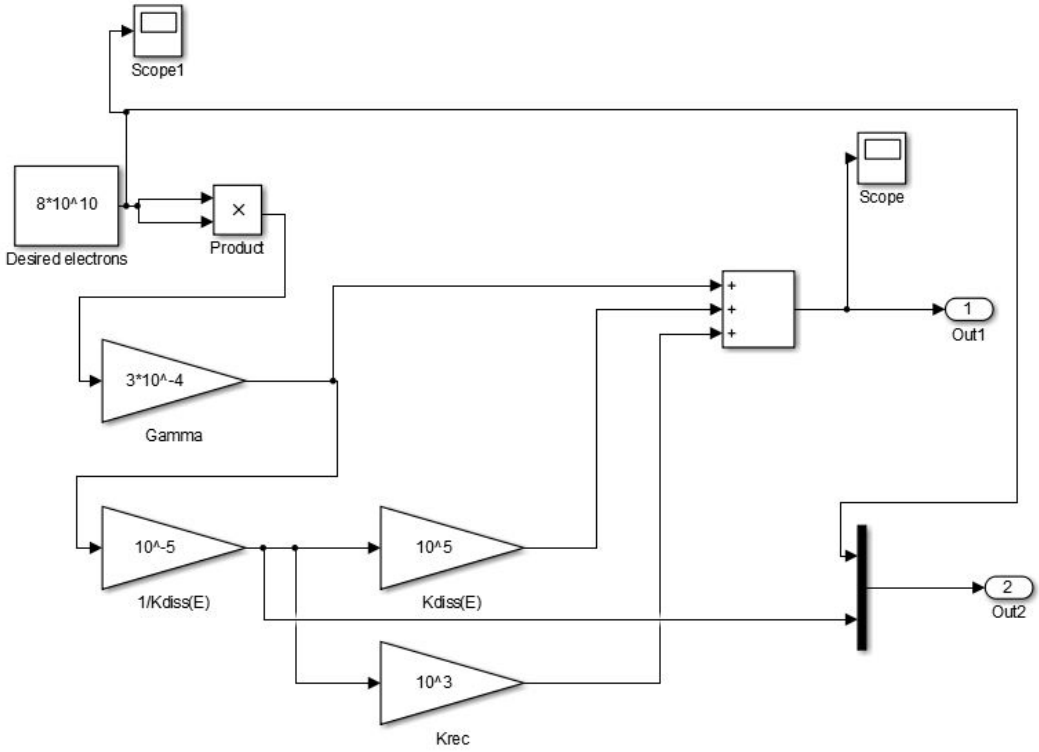

Figure 4.2: Solar Cell 2nd order Nonlinear Model : Set-point controller

As we know from Equation(3.47)

$$0 = u - k_{rec}x_2^{ss} - k_{diss}(E)x_2^{ss} - \gamma x_1^{2ss} \tag{4.1}$$

Thus, the set-point controller is given by :

$$u_{ss} = k_{rec}x_2^{ss} + k_{diss}(E)x_2^{ss} + \gamma x_1^{2ss} \tag{4.2}$$

which is represented above in Figure 4.2.

From Equation(3.46) :

$$0 = k_{diss}(E)x_2^{ss} - \gamma x_1^{2ss} \tag{4.3}$$

we get

$$x_2^{ss} = \frac{\gamma x_1^{2ss}}{k_d iss(E)} \tag{4.4}$$

4.2 Simulation Results of Frozen Space Submodel

Below the simulations results as simulated in MATLAB for a time period of 10^{-4} seconds.

4.2.1 Electrons : x_1

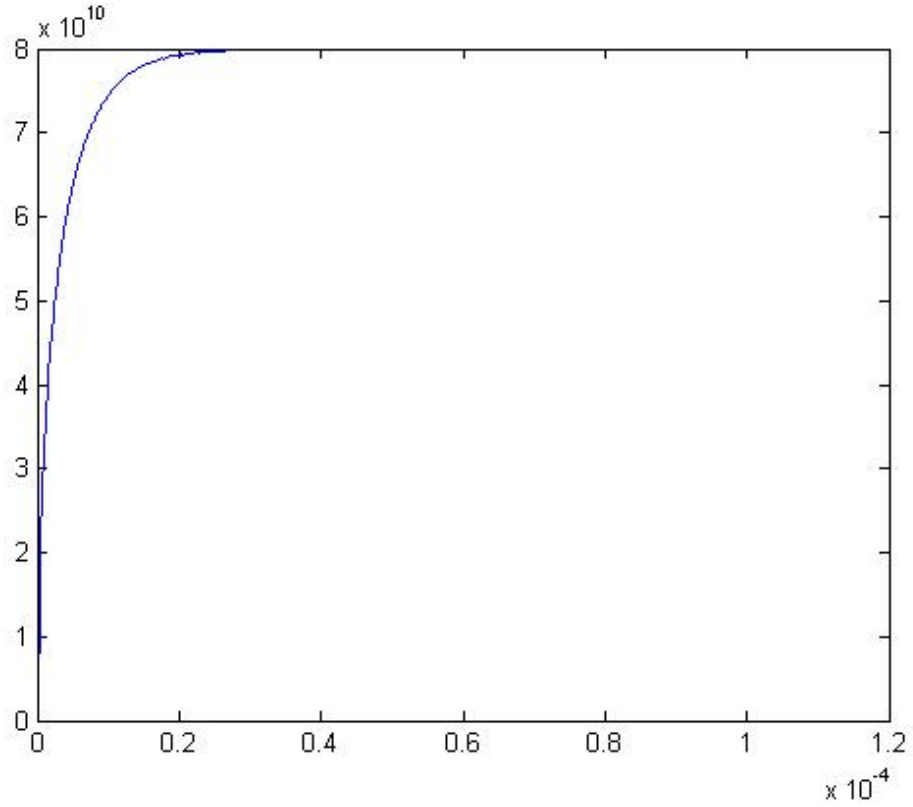

Figure 4.3: Solar cell 2nd order output y (number of electrons)

The above Figure 4.3 shows that the number of electrons is being maintained constant in this frozen time model.

Low Intensity

The input in our model is G, i.e the sunlight whose intensity can vary. The constant number of electrons will ensure in the event of low intensity that enough generated electrons are swept towards the cathode where they exit the device.

High Intensity

In the event of high intensity the biomolecular recombination factor k_{rec} is very strong. This recombination leads to a space charge effect which leads to the supression of an electric field in the device thereby essentially blocking the separation of electrons and holes from the excitons.

By maintaing a constant number of electrons the space charge effect can be somewhat supressed.

4.2.2 Charge Pairs : x_2

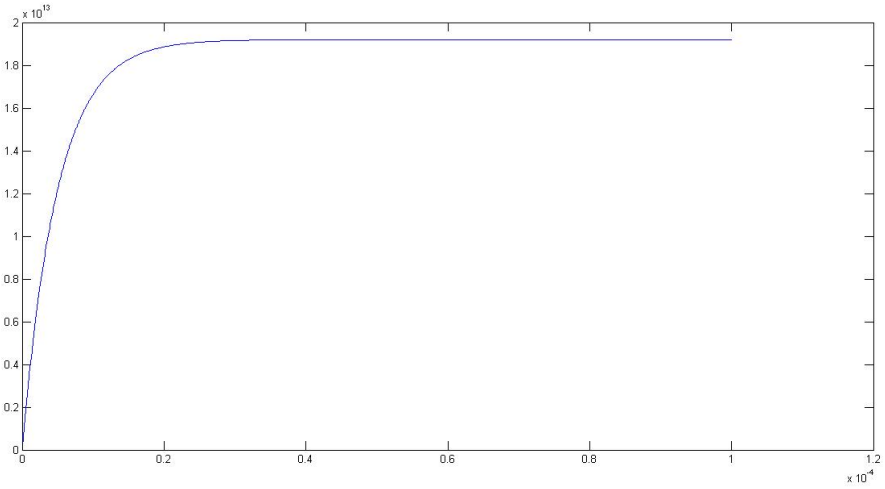

Figure 4.4: Solar cell 2nd order output (charge)

The above Figure 4.4 repsrented the dynamics of charge pairs as present in the device. In our sub-model (frozen space) we have achieved a steady charge pair of order 10^{13} units.

As concluded in [Hwang, 2008] the photocuurrent rise time in a bulk hetrojunction photovoltaic device is not solely associated with a carrier time, but also depends on the dynamics of charge pair seperation and recombination.

Low Intensity

A constant number of charge pairs in the event of low intensity will ensure that η_{diss} and η_{col} have high values and thereby overall affecting η_{eff} as also seen in Equation(2.5).

High Intensity

In the event of high intensity where biomolecular recombination is very strong, the charge pairs acts as a 'reservoir' which slows the passage of charge carriers but by controlling and maintaining a steady state of charge pairs we can somewhat diminish this effect. Thus a good value can be maintained for η_{diss} and this affects overall η_{eff}.

4.3 Frozen Time

In our submodel of frozen time we demonstrate the electrons and holes with their rate of change as they will vary inside the cell after the photons strile the cell. We try to replicate these sates as shown in the simulation diagrams (4.7), (4.8), (4.9), (4.10) of this model.

4.3.1 Data

The values of the parameter used to simulate the formulated model was obtained from Barker *et al.* [2003], [Hwang, 2008] and [Kirchartz *et al.*, 2008] :

$n : 1.6 * 10^{-}19\ C$ $\qquad$ $E = 7.1 * 10^{6}\ Vm^{-1}$

$K_{rec} = 10^{3}\ s^{-1}$ $\qquad$ $\mu_n = 3 * 10^{-10}\ m^2/Vs$

$\mu_p : 1 * 10^{-10}\ m^2/Vs$ $\qquad$ $G : 4.3 * 10^{17} m^{-3} s^{-1}$

Rest of paramaters are derived relationally (they are included in Apendix)

4.3.2 4th Order : Block Diagram

Figure 4.5 is a block diagram representation of the 4th order solar cell model in Simulink wherein a set point controller as shown in Figure 4.6 is used to control the number of electrons, rate of change of electrons, number of holes, and rate of change of holes as they will change inside the cell.

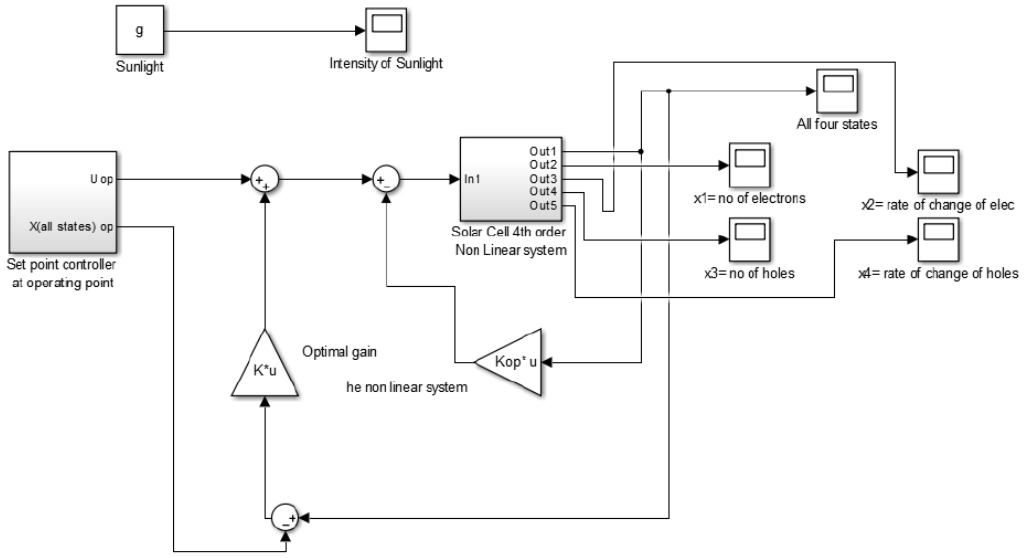

Figure 4.5: Solar cell 4th order Non Linear Model

4.3.3 Scaled Down Model

The original system matrix A is of the order of 10^{26} and B of the order of 10^{12}, which is numerically not ideal, thus we scale down the model for simulation purposes. The new parameters after scaling down are calculated as :

$$\hat{A} = 10^{-12}A, \hat{B} = 10^{-12}B, t = 10^{-12}\tau, u = 10^{6}\hat{u} \tag{4.5}$$

This scaled down system is numerically more stable and eaiser to simulate. This scaled down model is stabilizable and thus by applying the LQR optimal controller we are able to calculate the required gain to achieve our controller goal as discussed in Equation(3.45).

4.3.4 Set-Point Controller

As seen earlier in Section 3.4 for the 4th order model, the set-point controller cannot be achieved around the steady state point. Given the system matrix is of very high order in magnitude we calclulate the nominal operating points after performing some iterations in MATLAB.

Nominal operating point

Using MATLAB we calculated the values of operating points around which the system can be linearized

$$x_1^{op} = 706 \tag{4.6}$$

$$x_2^{op} = 2.63 * 10^7 \tag{4.7}$$

Using Equation(3.43) we get Equation(4.8)

$$x_3^{op} = \frac{g}{K_{rec}} \frac{1}{x_1^{ss}} \tag{4.8}$$

$$x_4^{op} = -1.22 * 10^8 \tag{4.9}$$

Also,

$$u^{op} = 10^7 * u \tag{4.10}$$

Thus, this is the set point controller which is shown below in Figure 4.6.

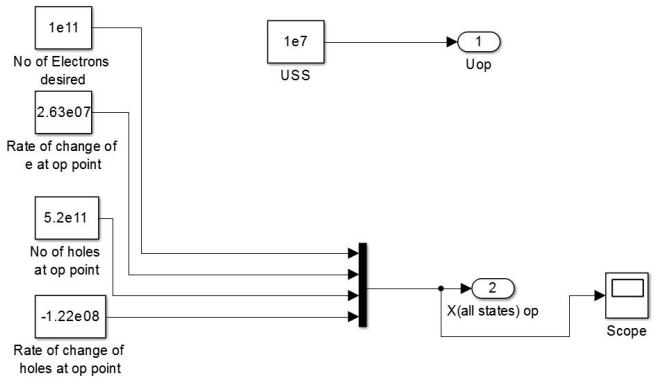

Figure 4.6: Solar cell 4th order Nonliinear Model : Set-point controller

4.4 Simulation Results of Frozen Time Submodel

By constructing the nonlinear model as seen in Figure 4.5 we are attempting to maintain a constant number of electrons as ideally the rate of flow of electrons determines the current. The model is simulated for a time period of 10^{-11} seconds.

4.4.1 Electrons : x_1

In this frozen time sub model we see that the number of electrons can be maintained constant in the order of desired 10^{11}.

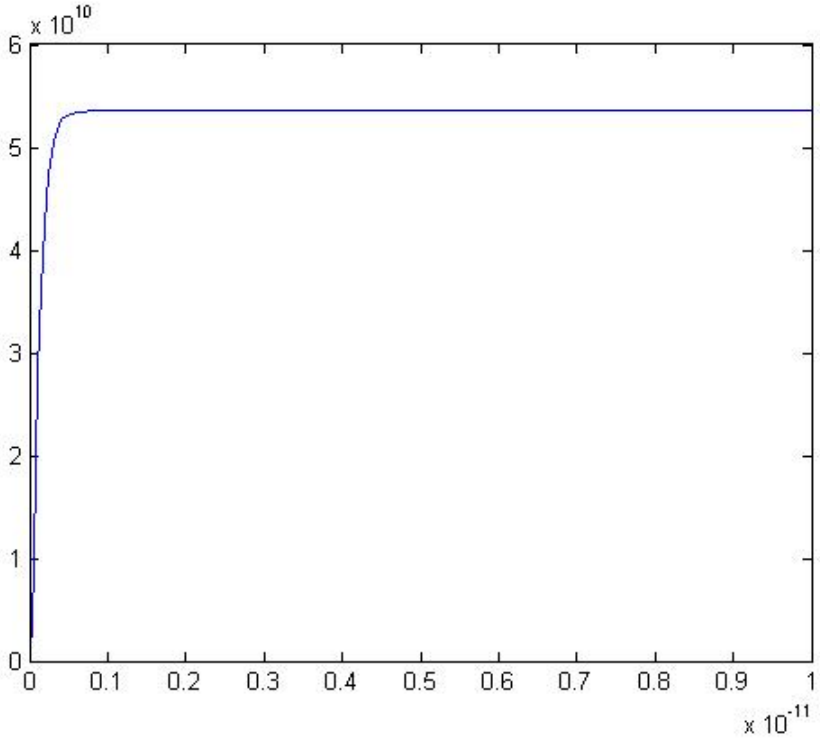

Figure 4.7: Solar cell 4th order output x_1 (number of electrons)

The input in our model is G, i.e the sunlight whose intensity can vary. The constant number of electrons as shown in Figure 4.7 will ensure in the event of low intensity that enough generated electrons are swept towards the cathode where they exit the device. In the event of high intensity the biomolecular recombination factor k_{rec} is very strong. This recombination leads to a space charge effect which leads to the supression of an electric field in the device thereby essentially blocking the separation of electrons and holes from the excitons. By maintaing a constant number of electrons the space charge effect can be supressed.

4.4.2 Rate of Change of Electrons : x_2

As shown in Figure 4.8 the rate of change of electrons can directly affect the output current

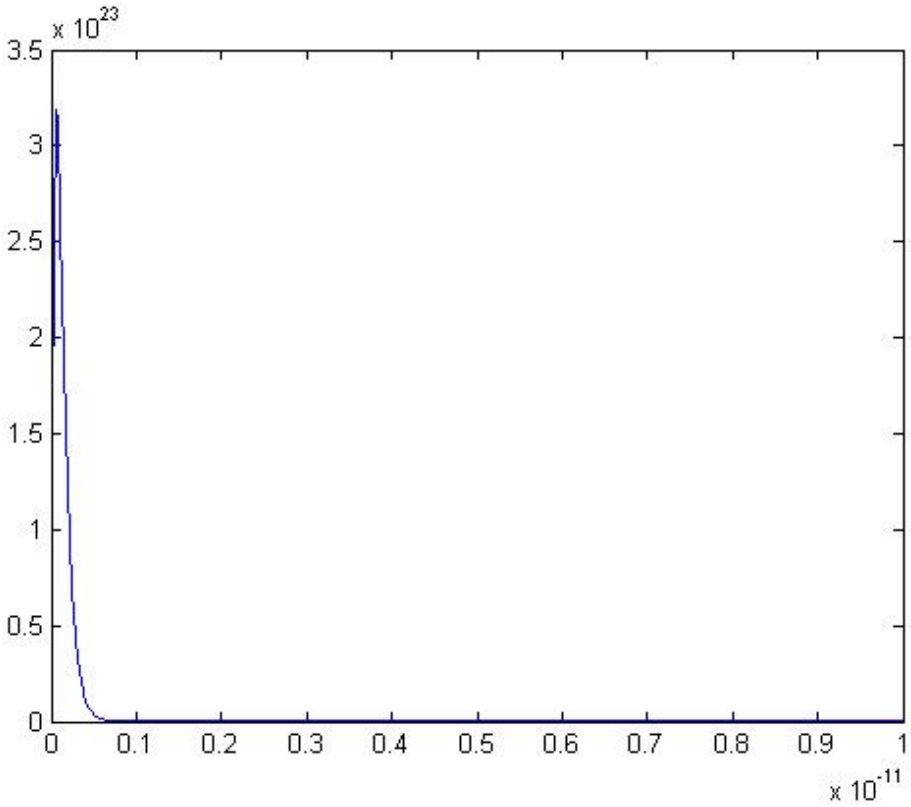

Figure 4.8: Solar cell 4th order output x_2 (rate of change of electrons)

4.4.3 Holes : x_3

The input in our model is G, i.e the sunlight whose intensity can vary. The constant number of holes as shown in Figure 4.9 will ensure in the event of low intensity that enough generated electrons are swept towards the anode where they exit the device. By maintaing a constant number of holes the space charge effect can be somewhat supressed.

4.4.4 Rate of Change of Holes : x_4

Around nominal operating point the rate of change in holes is shown in Fig 4.10.

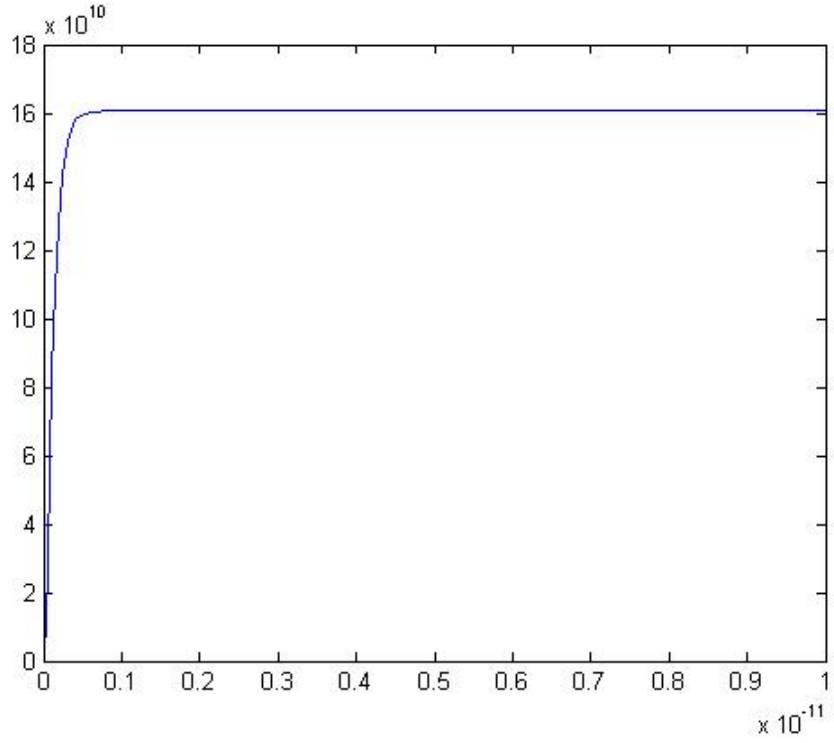

Figure 4.9: Solar cell 4th order output x_3 (number of holes)

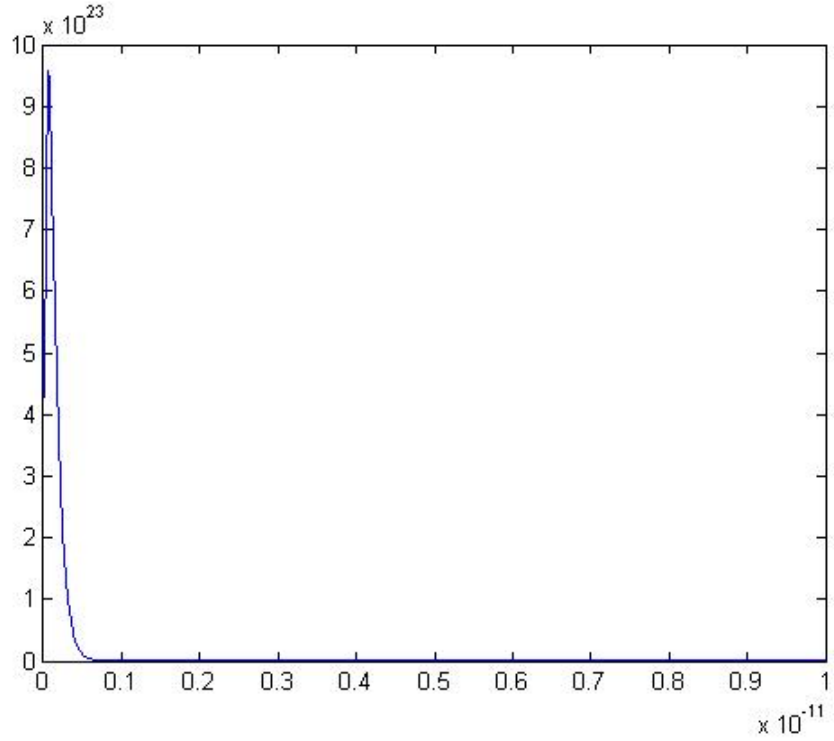

Figure 4.10: Solar cell 4th order output x_4 (rate of change of holes)

Chapter 5

Turing Patterns : Solar Cell Drift Diffusion Model

Turing's seminal work in 1952 [Turing, 1952] showed that for some non-linear reaction-diffusion equations the steady state solution of the system is not spatially uniform. The Turing instability occurs when a spatially homogeneous steady state of the reaction dynamics, which is linearly stable in the absence of diffusion, becomes linearly unstable when the reactions are coupled with the diffusion. This can occur when there are two or more nonlinearly interacting species with different diffusivites. The resultant inhomogeneous spatial pattern is called a Turing pattern [Stancevic *et al.*, 2013].

Turing argued that if the diffusion coefficients of the two species are widely different, then if one of the species is auto catalytic with the other inhibiting its growth, then the steady homogeneous state will be unstable to a patterned steady state. The instability could also set in as a temporal pattern in a spatially homogeneous state under certain conditions. Turing patterns have been a very important aspect of the study of the non linear systems.

As shown earlier in Equations(3.1), (3.2), (3.3), and (3.4), the solar cell model under inverstigation is varying with time also being spatially varying. Recently there has been extension of the Turing work in some unexpected directions and recently [Riaz *et al.*, 2004] have shown that a Turing pattern for charged species could be altered by an applied electric field. Thus, the spatio-temporal behaviour of this system is investigated within the framework of Turing instability-induced pattern formation.

5.1 Conditions for Fomation of Turing patterns

For any reaction diffusion systems spatially extended model patterns may occur in the neighbourhood of a spatially homogeneous steady state provided the conditions for a

Turing instability are met, namely that the spatially homogeneous steady state is:
($T1$) linearly stable in the absence of diffusion, and
($T2$) linearly unstable in the presence of diffusion.

5.2 Existence of Turing Patterns In Our Model

We need to investigate the dynamics of our time and space varying model whether it allows for formation of spatial patterns or not. A similar work for a two dimensioanl reaction model of HIV dynamics was carried out by [Stancevic *et al.*, 2013]. We have adapted their proposed approach and applied in our model.

5.3 Linearizing About Spatially Homogenous Steady State

The equations under investigation

$$\frac{\partial n}{\partial t} = k_{diss}(E)X - \gamma np \tag{5.1}$$

$$\frac{\partial p}{\partial t} = k_{diss}(E)X - \gamma np \tag{5.2}$$

$$\frac{\partial X}{\partial t} = G - k_{rec}X - k_{diss}(E)X - \gamma np \tag{5.3}$$

In these equations, the dependent variables are :
n : number of electrons in the solar cell; p : number of holes in the solar cell; and X : charge pairs formed in the exciton formation and disscoaition process, where these all vary with time t , but not space. The parameter $k_{diss}(E)$ represents dissociation of charge pairs, γ represents biomolecular recombination of electrons and holes to form charge pairs and k_{rec} represents dynamics of charge pairs which undergo molecular recombination.

Extending this model to include also spatial aspects so that the independent variables are now (t, z) produces the following model:

$$\frac{\partial n}{\partial t} = \frac{\partial}{\partial z}[-\mu_n k_B T \frac{\partial n}{\partial z} - \mu_n neE] + k_{diss}(E)X - \gamma np \tag{5.4}$$

$$\frac{\partial p}{\partial t} = \frac{\partial}{\partial z}[-\mu_p k_B T \frac{\partial p}{\partial z} + \mu_p neE] + k_{diss}(E)X - \gamma np \tag{5.5}$$

$$\frac{\partial X}{\partial t} = G - k_{rec}X - k_{diss}(E)X - \gamma np \tag{5.6}$$

To investigate further the above set of equations can be conveniently represented as :

$$\frac{\partial n}{\partial t} = -\alpha_n \frac{\partial^2 n}{\partial z^2} - \beta_n \frac{\partial n}{\partial z} + k_{diss}(E)X - \gamma np \tag{5.7}$$

$$\frac{\partial p}{\partial t} = -\alpha_p \frac{\partial^2 p}{\partial z^2} - \beta_p \frac{\partial p}{\partial z} + k_{diss}(E)X - \gamma np \tag{5.8}$$

$$\frac{\partial X}{\partial t} = G - k_{rec}X - k_{diss}(E)X - \gamma np \tag{5.9}$$

Now the linearized form for perturbation is given by :

$$\frac{\partial}{\partial \tau}\begin{bmatrix} \triangle n \\ \triangle p \\ \triangle X \end{bmatrix} = \begin{bmatrix} -\gamma p & -\gamma n & k_{diss}(E) \\ -\gamma p & -\gamma n & k_{diss}(E) \\ -\gamma p & -\gamma n & -k_{rec} - k_{diss}(E) \end{bmatrix} \begin{bmatrix} \triangle n \\ \triangle p \\ \triangle X \end{bmatrix} + \begin{bmatrix} 0 \\ 0 \\ G \end{bmatrix}$$
$$+ \begin{bmatrix} -\alpha_n & 0 & 0 \\ 0 & -\alpha_p & 0 \\ 0 & 0 & 0 \end{bmatrix} \begin{bmatrix} \frac{\partial^2 \triangle n}{\partial z^2} \\ \frac{\partial^2 \triangle p}{\partial z^2} \\ \frac{\partial^2 \triangle X}{\partial z^2} \end{bmatrix} + \begin{bmatrix} -\beta_n & 0 & 0 \\ 0 & \beta_p & 0 \\ 0 & 0 & 0 \end{bmatrix} \begin{bmatrix} \frac{\partial}{\partial z} \\ \frac{\partial}{\partial z} \\ \frac{\partial}{\partial z} \end{bmatrix}$$

After carrying out Fourier transforms with respect to the spatial variables yields :

$$\frac{\partial}{\partial \tau}\begin{bmatrix} \triangle n \\ \triangle p \\ \triangle X \end{bmatrix} = \begin{bmatrix} -\gamma p & -\gamma n & k_{diss}(E) \\ -\gamma p & -\gamma n & k_{diss}(E) \\ -\gamma p & -\gamma n & -k_{rec} - k_{diss}(E) \end{bmatrix} + \begin{bmatrix} \alpha_n q^2 & 0 & 0 \\ 0 & \alpha_p q^2 & 0 \\ 0 & 0 & 0 \end{bmatrix} + \begin{bmatrix} -jq\beta_n & 0 & 0 \\ 0 & jq\beta_p & 0 \\ 0 & 0 & 0 \end{bmatrix}. \tag{5.10}$$

where $\triangle N$, $\triangle P$, $\triangle X$ denote the Fourier transform of $\triangle n$, $\triangle p$ and $\triangle X$ respectively and $q^2 := q^T q$ where q $\in \Re^d$ is the Fourier variable, with d the spatial dimension.

Considering only the real part for the above equation gives us:

$$\frac{\partial}{\partial \tau}\begin{bmatrix}\triangle n\\ \triangle p\\ \triangle X\end{bmatrix} = \begin{bmatrix}-\gamma p + \alpha_n q^2 & -\gamma n & k_{diss}(E)\\ -\gamma p & -\gamma n + \alpha_p q^2 & k_{diss}(E)\\ -\gamma p & -\gamma n & -k_{rec} - k_{diss}(E)\end{bmatrix}\begin{bmatrix}\triangle N\\ \triangle P\\ \triangle X\end{bmatrix} \tag{5.11}$$

The conditions for Turing instabilities are determined from the eigenvalue spectrum of the coefficient matrix in Equation (5.11). The requirement that the homogeneous steady state is stable in the absence of diffusion is met if all eigenvalues have negative real parts when $q^2 = 0$. A Turing instability may then occur if one or more eigenvalues have positive real parts for some $q^2 > 0$.

The characteristic polynomial of the matrix in Equation (5.11)

$$A = \begin{bmatrix}-\gamma p + \alpha_n q^2 & -\gamma n & k_{diss}(E)\\ -\gamma p & -\gamma n + \alpha_p q^2 & k_{diss}(E)\\ -\gamma p & -\gamma n & -k_{rec} - k_{diss}(E)\end{bmatrix} \tag{5.12}$$

is calculated by

$$\triangle(\lambda) = det(\lambda I - A) \tag{5.13}$$

$$\triangle(t) = det\begin{bmatrix}\lambda + \gamma p - \alpha_n q^2 & \gamma n & -k_{diss}(E)\\ \gamma p & \lambda + \gamma n - \alpha_p q^2 & -k_{diss}(E)\\ \gamma p & \gamma n & \lambda + k_{rec} + k_{diss}(E)\end{bmatrix} \tag{5.14}$$

The determinant of the matrix in Equation (5.14) gives us the following form :

$$\lambda^3 + \lambda^2[k_{rec} + k_{diss}(E) + \gamma n - \alpha_p q^2 + \gamma p - \alpha_n q^2] + \lambda[k_{rec}\gamma n + k_{diss}(E)\gamma n - k_{rec}\alpha_p q^2 - k_{diss}(E)\alpha_p q^2 + k_{diss}(E)\gamma n + k_{rec}\gamma p + k_{diss}(E)\gamma p - \alpha_p q^2\gamma p + k_{diss}(E)\gamma p] + [-k_{rec}\alpha_p q^2\gamma p - k_{diss}(E)\alpha_p q^2\gamma p - \alpha_n q^2 k_{rec}\gamma n - \alpha_n q^2 k_{diss}(E)\gamma n + k_{rec}\alpha_n\alpha_q q^4 + k_{diss}(E)\alpha_n\alpha_q q^4 - \alpha_n\gamma n k_{diss}(E)q^2 - k_{diss}(E)\alpha_p q^2] = 0$$

. (5.15)

To check for stability, recall that a cubic polynomial $\lambda^3+a\lambda^2+b\lambda+c$ has all roots in the left half complex plane if and only if $a, b, c > 0$ and $ab > c$ (Routh-Hurwitz stability criterion for a cubic polynomial) [Hurwitz, 1964]. Below we consider the characteristic polynomial for different values of q^2.

5.3.1 Case of No Spatial Variation

In the absence of diffusion ($q^2 = 0$), the characteristic polynomial Equation A simplifies to

$$\lambda^3+\lambda^2[k_{rec}+k_{diss}(E)+\gamma n+\gamma p]+\lambda[k_{rec}\gamma n+k_{rec}\gamma p+2k_{diss}(E)\gamma n+2k_{diss}(E)\gamma p] \quad (5.16)$$

Since the parameters are positive all the coefficients of Equation (5.16) are positive and this case is essentially the same as our Frozen Space model. Now the remaining condition

$$(k_{rec} + k_{diss}(E) + \gamma n + \gamma p)(k_{rec}\gamma n + k_{rec}\gamma p + 2k_{diss}(E)\gamma n + 2k_{diss}(E)\gamma p) > 0 \quad (5.17)$$

is necessary and sufficient for all roots of (5.16) to be in the left half plane.

Thus, the endemic steady state is stable in the absence of diffusion and the first Turing condition ($T1$) is satisfied. We can also conclude from the relation as shown in Equations (3.60) and (3.61) that in case of no spatial variation the system is asymptotically stable.

5.3.2 Case of Spatial Variation

Now we investigate the nature of the roots of Equation (5.15) in the presence of diffusion ($q^2 = 0$).

Firstly, consider the case for large q^2. Then the coefficients of characteristic polynomial (5.15) will determine the inherent stability of the system. The Equation (5.15) can be conveniently represnted as :

$$\lambda^3+\lambda^2[k_{rec}+k_{diss}(E)+\gamma n+\gamma p-(\alpha_p+\alpha_n)q^2]+\lambda[k_{rec}\gamma n+2k_{diss}(E)\gamma n+k_{rec}\gamma p+2k_{diss}(E)\gamma p-(k_{rec}\alpha_p+\alpha_p\gamma p+k_{diss}(E)\alpha_p)q^2]+[(k_{rec}\alpha_n\alpha_q+k_{diss}(E)\alpha_n\alpha_q)q^4-(k_{rec}\alpha_p\gamma p+k_{diss}(E)\alpha_p\gamma p+\alpha_n k_{rec}\gamma n+2\alpha_n k_{diss}(E)\gamma n+k_{diss}(E)\alpha_p)q^2]$$

. (5.18)

To investigate the stability the above Equation (5.18) can also be conveniently reprsented as :

$$\lambda^3+\lambda^2(a_1-a_2q^2)+\lambda(b_1-b_2q^2)+(c_1q^4-c_2q^2) \tag{5.19}$$

Investigation of Roots :

Firstly, consider the case for large q^2. Then the characteristic polynomial shown in Equation(5.15) will have all its coefficients positive (as in each term the largest power of q^2 has a positive coefficient). It is then straightforward to show that the product of the former two is larger than the latter, hence for sufficiently large q^2 all roots of Equation (5.15) are in the left half complex plane and the syetem is stable.

Even though for large values of q^2 the system becomes stable, there may still be an appropriate range of values of q^2 for which instabilities occur. As we note from Equation (5.19) that all coefficients are positive except for possibly a_2, b_2, c_2. If we assume if these too are positive then :

$$\lambda^3+\lambda^2(a_1+a_2q^2)+\lambda(b_1+b_2q^2)+(c_1q^4+c_2q^2) \tag{5.20}$$

As we know from [Hurwitz, 1964] $ab > c$, thus we get the following conditions :

$$(S1) \quad a_1b_2+a_2b_1>c_2 \qquad\qquad (S2) \quad a_2b_2>c_1 \tag{5.21}$$

Proof of $S2$:

$$(\alpha_n+\alpha_q)(k_{rec}\alpha_p+k_{diss}(E)\alpha_p+\alpha_p\gamma p)>k_{rec}\alpha_n\alpha_q+k_{diss}(E)\alpha_n\alpha_q \tag{5.22}$$

Clearly on expansion of Equation (5.22) above equality holds and thus $S2$ holds true.

Proof of $S1$:

To satsify the inequality as shown in Equation (5.21) is not possibe as the combination of parameters is different on both sides of the inequality i.e. $S1$ does not hold. Thus, we can conclude that in case of spatial variation the model is linearly unstable in the neighbourhood of spatially homogeneous steady state.

5.4 Conclusion

As discussed in Section 5.1 that for the existence of Turing patterns the Turing instability conditions must be met namely :
($T1$) linearly stable in the absence of diffusion, and
($T2$) linearly unstable in the presence of diffusion.

We have proved both the above conditions as seen in case of both no spatial variation and in the case of spatial variation respectively. Thus, we can conclude about the exostence of Turing patterns in our model.

Chapter 6

Thesis Conclusion and Future Research Work

6.1 Conclusions

The study of control techniques for organic solar cells are investigated in this thesis. The organic solar cell (OSC) which is a promising candidate in the PV industry needs to be studied well. We analyzed the various parameters which play a major role in the conversion of photovoltaic current after sunlight falls on the OSC.

We studied the one dimensional drift diffusion equation which explains the internal physics of an OSC. We further took the space and time varying differential equations and modelled them into two sub-models : by freezing space and by freezing time. We checked the internal stability of this two models by subjecting them to the Routh-Hurwitz stability test and found them to be asymtotically stable. Using linear quadratic optimal controller and setpoint controller we were able to maintain the constant number of electrons and charge pairs around the operating point of the considered nonlinear model.

We discussed the results of simulation and made observations as to how these results relate to the performance of the cell in varying sunlight. In addition, we subjected our model to the Turing pattern instabiliy test to confirm the presence of Turing patterns from a reaction diffusion system point of view.

6.2 Future Work

In the future, we plan to develop a state space form of equations for the original nonlinear model. Then, we can design a nonlinear controller to control the useful parameters of the organic solar cell. The new simulated model will be then very close

to reality.

Since the organic solar cell is very complex in nature from a physics point of view which involves huge range of parameters, drift diffusion equations may be studied more in detail and corresponding controllers can be designed in the future using multiple time scales.

We can also coordinate with the material people and can share our results which can help them choose the organic materials keeping in mind the consideration of parameters and how they affects the performance.

References

Alon, U. (2008). *Organic Semiconductors for Low-Cost Solar Cells*. Chapman & Hall/CRC Mathematical & Computational Biology, Boca Raton, FL, USA.

Arkhipov, V.I., Heremans, P., and Bssler, H. (2003). Why is exciton dissociation so efficient at the interface between a conjugated polymer and an electron acceptor? *Applied Physics Letters*, 82(25).

Barker, J.A., Ramsdale, C.M., and Greenham, N.C. (2003). Modeling the current-voltage characteristics of bilayer polymer photovoltaic devices. *Phys. Rev. B*, 67, 075205. doi:10.1103/PhysRevB.67.075205. URL `http://link.aps.org/doi/10.1103/PhysRevB.67.075205`.

Crabtree, G.W. and Lewis, N.S. (2007). Solar energy conversion. *Physics today*, 60(3), 37–42.

Davoudi, A., Jatskevich, J., Chapman, P., and Bidram, A. (2013). Multi-resolution modeling of power electronics circuits using model-order reduction techniques. *Circuits and Systems I: Regular Papers, IEEE Transactions on*, 60(3), 810–823. doi: 10.1109/TCSI.2012.2215745.

Dorato, P., Cerone, V., and Abdallah, C. (2000). *Linear Quadratic Control: An Introduction*. Krieger Publishing Co., Inc., Melbourne, FL, USA.

EPIA (2013). Global market outlook for photovoltaics until 2014.

Friedland, B. (1985). *Control Systems Design: An Introduction to State-Space Methods*. McGraw-Hill Higher Education.

Gajic, Z. (2003). *Linear dynamic systems and signals*. Prentice Hall/Pearson Education.

Hurwitz (1964). On the conditions under which an equation has only roots with negative real parts. 72–82.

Hwang, C.K., Huang, K.S., Lin, K.B., and Lee, B.K. (2010). Observer base linear quadratic regulation with estimated state feedback control. In *Machine Learning and Cybernetics (ICMLC), 2010 International Conference on*, volume 6, 2802–2805. doi:10.1109/ICMLC.2010.5580791.

Hwang, N.G. (2008). Modelling photocurrent transients in organic solar cells. *Nanotechnology 19 424012*.

Iyer, S. and Subramanian, V. (2007). Tutorial t2: Organic electronics: Technology, devices, circuits, and applications. 4–4. doi:10.1109/VLSID.2007.166.

Kirchartz, T., Pieters, B., Taretto, K., and Rau, U. (2008). Electro-optical modeling of bulk heterojunction solar cells. *Journal of Applied Physics*, 104(9), 094513–094513–9. doi:10.1063/1.3013904.

McGehee, Michael D.; Goh, C. (2008). Organic semiconductors for low-cost solar cells. *PHYSICS OF SUSTAINABLE ENERGY: Using Energy Efficiently and Producing It Renewably. AIP Conference Proceedings*, 138(4), 322–330.

Riaz, S.S., Kar, S., and Ray, D.S. (2004). Mobility-induced instability and pattern formation in a reaction-diffusion system. *The Journal of Chemical Physics*, 121(11).

Selwan, E. (2012). *Control Strategies for Power Converters used on Solar Cells*. Master's thesis, Rutgers University, USA.

Servaites, J.D., Ratner, M.A., and Marks, T.J. (2011). Organic solar cells: A new look at traditional models. *Energy Environ. Sci.*, 4, 4410–4422. doi:10.1039/C1EE01663F. URL `http://dx.doi.org/10.1039/C1EE01663F`.

Stancevic, O., Angstmann, C.N., Murray, J.M., and Henry, B.I. (2013). Turing patterns from dynamics of early hiv infection. *Bull Math Biol*. URL `http://www.biomedsearch.com/nih/Turing-Patterns-from-Dynamics-Early/23546926.html`.

Turing, A. (1952). The chemical basis of morphogenesis. *Philosophical Transactions of the Royal Society B*, 237, 37–72.